Eur. Phys. J. C 48, 135–145 (2006)
Digital Object Identifier (DOI) 10.1140/epjc/s10052-006-0013-9

THE EUROPEAN PHYSICAL JOURNAL C

Theoretical Physics

Hadron-pair photoproduction in longitudinally polarized lepton–nucleon collisions

C. Hendlmeier[a], M. Stratmann[b], A. Schäfer

Institut für Theoretische Physik, Universität Regensburg, 93040 Regensburg, Germany

Received: 9 June 2006 /
Published online: 28 September 2006 –

Abstract. We present a detailed phenomenological study of photoproduction of two hadrons, both with high-transverse momentum, in longitudinally polarized lepton–nucleon collisions. We consistently include "direct" and "resolved" photon contributions and examine the sensitivity of the relevant spin asymmetries to the gluon polarization in the nucleon and to the completely unknown parton content of circularly polarized photons. Our results are relevant for the COMPASS and HERMES fixed-target experiments as well as for a possible future polarized lepton–proton collider like eRHIC at BNL. So far, all studies are limited to the lowest order approximation of QCD.

PACS. 13.88.+e; 12.38.Bx; 13.85.Ni

1 Motivation and introduction

The fundamental question of how the spin of the proton is composed of the spins and orbital angular momenta of its constituents, quarks and gluons, still remains unanswered. Over the past 25 years, a series of polarized deep-inelastic scattering (DIS) experiments have revealed that the quark spins contribute remarkably little to the nucleon spin [1]. Measuring $\Delta g(x,\mu)$, the spin-dependent gluon distribution in the nucleon, in an as large as possible range of momentum fractions x, is the prime goal of all current experiments with polarized beams and targets. In the light-cone gauge the first moment of $\Delta g(x,\mu)$, i.e. $\int_0^1 \Delta g(x,\mu)\mathrm{d}x$, can be interpreted as the gluon spin contribution to the nucleon spin at a momentum scale μ [2]. The missing piece, the orbital angular momenta of quarks and gluons, might be accessible in exclusive processes, but precise measurements are challenging and rather distant at this point.

The advent of the Relativistic Heavy Ion Collider (RHIC) at Brookhaven National Laboratory (BNL), has opened up unequaled possibilities to access Δg over a broad range in x in a variety of high-transverse momentum, "high-p_{T}", processes such as, for example, inclusive hadron or jet, prompt photon, and heavy flavor production [3, 4]. In each case, the gluon density prominently contributes through gluon–gluon fusion and quark–gluon scattering processes already at the lowest order (LO) approximation of QCD. Center-of-mass system (c.m.s.) energies of up to $\sqrt{S} = 500\,\mathrm{GeV}$ guarantee that the standard framework of perturbative QCD (pQCD) can be used reliably to learn about all aspects of helicity-dependent parton densities at RHIC. A series of unpolarized "benchmark" measurements at RHIC has nicely confirmed the applicability of pQCD methods [5–10] and is the foundation for similar, ongoing measurements with polarization. First, very recent results from the PHENIX and STAR collaborations at RHIC [11–14] indicate that large and positive gluon distributions are disfavored in the range of momentum fractions x, $0.03 \lesssim x \lesssim 0.2$, dominantly probed in these experiments. Future more precise measurements will extend the range in x and further close in on Δg.

The gluon polarization can be accessed also in low energy fixed-target experiments like COMPASS [15] at CERN and HERMES [16] at DESY. Here one scatters a beam of longitudinally polarized leptons off longitudinally polarized nucleons at c.m.s. energies of $\sqrt{S} \simeq 18\,\mathrm{GeV}$ and $\sqrt{S} \simeq 7.5\,\mathrm{GeV}$, respectively. Compared to RHIC, $\Delta g(x,\mu)$ is probed in a more limited x-range, $0.1 \lesssim x \lesssim 0.2$, but at smaller momentum scales μ, which makes results complementary. In particular, high-p_{T} hadron pairs, both in photoproduction and in deep-inelastic electroproduction, have been identified to be the most promising processes for a determination of Δg at the low energies available at fixed-target experiments [17]. First results for double-spin asymmetries are available from HERMES [18]

[a] e-mail: christof.hendlmeier@physik.uni-regensburg.de
[b] Address since August 15th, 2006: Radiation Laboratory, RIKEN, Wako, Saitama 351-0198, Japan

(for all photon virtualities), SMC [19] (electroproduction), and, most recently, COMPASS [20] (photoproduction). These data are consistent with only moderate gluon polarizations, as we will discuss in detail later.

However, at the smaller c.m.s. energies of fixed-target experiments it is much less obvious that standard pQCD methods are applicable as straightforwardly as at collider energies to analyze data. In fact, experimental results for high-p_{T} processes in, e.g., hadron–hadron fixed-target scattering have been a serious challenge in the past for the standard factorized framework where the perturbative series is truncated at a given fixed order in the strong coupling and where possible power corrections are assumed to be negligible [21–25]. It is therefore crucial to demonstrate *first* that standard pQCD methods can be used to learn about the parton and/or spin content of nucleons in a given kinematical regime, for instance, by analyzing unpolarized cross sections. Otherwise conclusions about, e.g., the gluon polarization might be incorrect.

In this paper we present a detailed phenomenological study of photoproduction of hadron pairs at LO accuracy of QCD. Quasi-real photons have the advantage of yielding much higher rates than deeply-inelastic electroproduction of hadrons. The price to pay is the more involved theoretical framework for photoproduction, where so-called "direct" and "resolved" photons contribute to the cross section as depicted in Fig. 1a and b, respectively. In Fig. 1a the photon simply interacts as an elementary pointlike particle, whereas in the latter case the photon "resolves" into its parton content prior to the hard QCD interaction, for instance, by fluctuating into a vector meson with the same quantum numbers. Here, cross section estimates require knowledge of the parton content of circularly polarized photons, which is lacking completely at the moment. We will demonstrate below that this does not seriously limit the usefulness of this process for the kinematical region specific to both COMPASS and HERMES. Since the theoretical framework for hadron-pair production is significantly more complex than for single-inclusive cross sections, next-to-leading order (NLO) QCD corrections are still not complete in the polarized case at the moment [26]. We note that there had been earlier studies of hadron-pair production [27–29] in the wake of first experimental results from HERMES [18]. However, the phenomenological results presented in [27–29] cannot be compared easily with the recent (and upcoming) results from COMPASS [20] we are aiming at.

Investigations of interactions between polarized leptons and nucleons will, hopefully, continue to play a vital role in spin physics also in the future. A polarized lepton–nucleon collider such as the eRHIC project at BNL [30, 31], which is currently under discussion, would be the next logical step. Besides the unique possibility to access $\Delta g(x,\mu)$ down to $x \simeq 10^{-3}$ in studies of scaling violations in DIS, photoproduction processes are particularly interesting also at collider energies [32]. As we shall show below, they will allow one to probe for the first time different models for the parton content of circularly polarized photons.

The paper is organized as follows: in Sect. 2 we briefly recall the theoretical framework for photoproduction of hadron pairs. Section 3 is devoted to detailed phenomenological studies. Here we mainly focus on the COMPASS and HERMES experiments, where first data are already available. We present results for spin asymmetries and discuss their possible sensitivity to Δg but also focus on predictions for unpolarized reference or "benchmark" cross sections which allow one to probe the validity of the pQCD framework at low c.m.s. energies and transverse momenta p_{T}. We include all relevant experimental cuts in our calculations. We close this section by studying the prospects for hadron-pair photoproduction at eRHIC. We briefly conclude in Sect. 4.

2 Technical framework

We consider the spin-dependent inclusive photoproduction cross section for the process

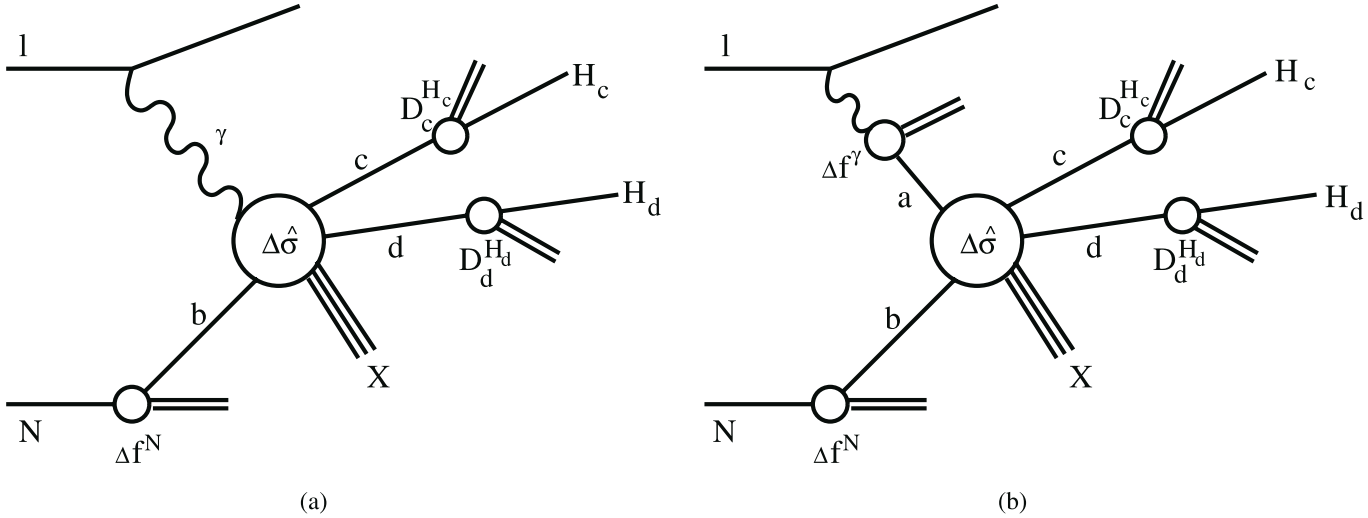

Fig. 1. Generic direct **a** and resolved **b** photon contributions to the photoproduction of a pair of hadrons H_c and H_d

$$l(p_l)N(p_N) \to l'(p_{l'})\, H_c(p_c)\, H_d(p_d)X\,, \tag{1}$$

where a longitudinally polarized lepton beam l scatters off a longitudinally polarized nucleon target N producing two observed hadrons H_c and H_d in the final state. The p_i denote the four-momenta of the particles. Both hadrons H_c and H_d are assumed to have high-transverse momenta $p_{\mathrm{T},c}$ and $p_{\mathrm{T},d}$, respectively, ensuring large momentum transfer. Invoking the factorization theorem [33–41] we may then write the differential cross section as a convolution of the non-perturbative parton distribution and fragmentation functions and partonic hard scattering cross sections,

$$\begin{aligned} \mathrm{d}\Delta\sigma &\equiv \frac{1}{2}[\mathrm{d}\sigma_{++} - \mathrm{d}\sigma_{+-}] \qquad (2)\\ &= \sum_{abcd} \int \mathrm{d}x_a\, \mathrm{d}x_b\, \mathrm{d}z_c\, \mathrm{d}z_d\, \Delta f^l(x_a,\mu_\mathrm{f})\, \Delta f^N(x_b,\mu_\mathrm{f}) \\ &\quad \times \mathrm{d}\Delta\hat{\sigma}^{ab\to cdX'}(S, x_a, x_b, p_c/z_c, p_d/z_d, \mu_\mathrm{f}, \mu'_\mathrm{f}, \mu_\mathrm{r}) \\ &\quad \times D_c^{H_c}(z_c,\mu'_\mathrm{f})\, D_d^{H_d}(z_d,\mu'_\mathrm{f})\,. \qquad (3) \end{aligned}$$

In (2) the subscripts "++" and "+−" denote the helicities of the colliding leptons and nucleons. S is the total c.m.s. energy squared available, i.e., $S = (p_l + p_N)^2$. The sum in (3) runs over all possible partonic channels $ab \to cd$, with $\mathrm{d}\Delta\hat{\sigma}^{ab\to cd}$ the associated spin-dependent LO partonic hard scattering cross sections. The latter can be calculated in pQCD order-by-order in the strong coupling $\alpha_\mathrm{s}(\mu_\mathrm{r})$, with μ_r denoting the renormalization scale.

The $\Delta f^N(x_b,\mu_\mathrm{f})$ are the usual spin-dependent parton distributions of the nucleon,

$$\Delta f^N(x_b,\mu_\mathrm{f}) = f_+^N(x_b,\mu_\mathrm{f}) - f_-^N(x_b,\mu_\mathrm{f})\,, \tag{4}$$

evolved to a factorization scale μ_f, with x_b the momentum fraction of the nucleon carried by the parton f. The subscript + [−] in (4) indicates that the parton's spin is aligned [anti-aligned] to the spin of the parent nucleon. The other non-perturbative functions $D_{c,d}^{H_{c,d}}(z_{c,d},\mu'_\mathrm{f})$ describe the collinear fragmentation of the partons c and d into the observed hadrons H_c and H_d, respectively, with $z_{c,d}$ the fraction of the parton's momentum carried by the produced hadron. μ'_f denotes the final-state factorization scale which can be different from μ_f.

The experimentally measured cross section for (1) is the sum of the so-called "direct" and "resolved" photon contributions, cf. Fig. 1a and b, respectively,

$$\mathrm{d}\Delta\sigma = \mathrm{d}\Delta\sigma_\mathrm{dir} + \mathrm{d}\Delta\sigma_\mathrm{res}\,. \tag{5}$$

We shall note that neither $\mathrm{d}\Delta\sigma_\mathrm{dir}$ nor $\mathrm{d}\Delta\sigma_\mathrm{res}$ are measurable individually. Both $\mathrm{d}\Delta\sigma_\mathrm{dir}$ and $\mathrm{d}\Delta\sigma_\mathrm{res}$ can be cast into the form of (3) by appropriately defining the parton distribution functions for a lepton, $\Delta f^l(x_a,\mu_\mathrm{f})$. Most generally, they can be written as convolutions,

$$\Delta f^l(x_a,\mu_\mathrm{f}) = \int_{x_a}^1 \frac{\mathrm{d}y}{y} \Delta P_{\gamma l}(y)\, \Delta f^\gamma\left(x_\gamma = \frac{x_a}{y}, \mu_\mathrm{f}\right)\,, \tag{6}$$

with

$$\begin{aligned} \Delta P_{\gamma l}(y) = \frac{\alpha_\mathrm{em}}{2\pi} \Bigg[&\frac{1-(1-y)^2}{y} \ln \frac{Q^2_\mathrm{max}(1-y)}{m_l^2 y^2} \\ &+ 2m_l^2 y \left(\frac{1}{Q^2_\mathrm{max}} - \frac{1-y}{m_l^2 y^2}\right)\Bigg] \end{aligned} \tag{7}$$

being the spin-dependent Weizsäcker–Williams equivalent photon spectrum [42] that describes the collinear emission of a quasi-real photon with momentum fraction y and virtuality less than some (small) upper limit Q_max off a lepton of mass m_l. Q_max is determined by the experimental conditions.

The explicit form of the polarized photon structure function $\Delta f^\gamma(x_\gamma,\mu)$ in (6) depends on the specifics of the interaction that the quasi-real photon undergoes in the hard scattering with the nucleon. In the "direct" case, depicted in Fig. 1a, parton a in (3) has to be identified with an elementary photon and hence x_a with the momentum fraction y of the photon with respect to the parent lepton, i.e.,

$$\Delta f^\gamma(x_\gamma,\mu) = \delta(1-x_\gamma) \tag{8}$$

in (6). If the photon resolves into its hadronic structure before the hard scattering takes place, the Δf^γ in (6) represent the parton densities of a circularly polarized photon. The latter are defined in complete analogy to the ones for a nucleon target in (4). Unlike hadronic parton distributions, photonic densities consist of a perturbatively calculable "pointlike" contribution, which dominates their behavior at large momentum fractions x_γ, and a non-perturbative "hadronic" contribution dominating in the low-to-mid x_γ region. Nothing is known about the latter, such that we have to invoke some model for it in our calculations below. This will become important in the discussion of the numerical results in the remainder of the paper. We will demonstrate that measurements at low c.m.s. energies, i.e., at COMPASS and HERMES, are to a large extent not affected by the actual details of the model. At higher c.m.s. energies, like at a future polarized ep collider, one of the physics goals would be a first determination of the partonic structure of circularly polarized photons.

Finally, the experimentally relevant double-spin asymmetry A_LL is defined as

$$A_\mathrm{LL} \equiv \frac{\mathrm{d}\Delta\sigma}{\mathrm{d}\sigma} = \frac{\mathrm{d}\sigma_{++} - \mathrm{d}\sigma_{+-}}{\mathrm{d}\sigma_{++} + \mathrm{d}\sigma_{+-}}\,. \tag{9}$$

The required spin-averaged cross section $\mathrm{d}\sigma$ in (9) is straightforwardly obtained from (3)–(7) by replacing all polarized quantities by their appropriate unpolarized counterparts.

3 Phenomenological applications

In our phenomenological studies based on the framework laid out in (3)–(7) we concentrate on the production of pairs of charged hadrons made of light quark flavors. In fact, we sum over pions, kaons, and (anti-) protons and

use the fragmentation functions of KKP [43] throughout to model hadronization. All our results will be differential in the transverse momentum $p_{\mathrm{T},c}$ of the hadron H_c and integrated over all kinematically and experimentally allowed transverse momenta $p_{\mathrm{T},d}$ of the hadron H_d and pseudo-rapidities $\eta_{c,d}$, unless stated otherwise. The pseudo-rapidities of the hadrons are measured with respect to the direction of the incident lepton beam.

For the unpolarized parton densities of the nucleon and photon we adopt the LO CTEQ6L [44] and GRV [45] sets, respectively. To study the sensitivity to the unknown gluon polarization of the nucleon we use four different sets of spin-dependent parton distributions emerging from the GRSV analysis [46]. These sets span a rather large range of gluon densities Δg, all very much consistent with present DIS data. Apart from our default "standard" set of GRSV with a moderately large, positive Δg, the three other sets "$\Delta g = g$ input", "$\Delta g = 0$ input", and "$\Delta g = -g$ input" are characterized by a large positive, a vanishing, and a large negative gluon polarization, respectively, at the input scale of the evolution.

The unknown parton densities of circularly polarized photons are estimated with the help of two extreme models [47–50] based on maximal, $\Delta f^{\gamma}(x,\mu_0) = f^{\gamma}(x,\mu_0)$, or minimal, $\Delta f^{\gamma}(x,\mu_0) = 0$, saturation of the positivity bound at the starting scale μ_0 for the evolution to scales $\mu > \mu_0$. Both models result in very different parton distributions Δf^{γ} at small-to-medium x_{γ}, while they almost coincide as $x_{\gamma} \to 1$ due to the dominance of the perturbatively calculable "pointlike" contribution in this region. The use of the "maximal" set will be implicitly understood except when we study the sensitivity of the photoproduction cross sections and spin asymmetries to the details of the non-perturbative hadronic input to the evolution of Δf^{γ}.

Unless stated otherwise, all factorization and renormalization scales, μ_{f}, μ'_{f}, and μ_{r}, in (3) are set equal to $\mu^2 \equiv \mu_{\mathrm{r}}^2 = \mu_{\mathrm{f}}^2 = \mu_{\mathrm{f}}'^2 = p_{\mathrm{T},c}^2 + p_{\mathrm{T},d}^2$.

3.1 Two-hadron production at COMPASS

With the present setup, the COMPASS experiment scatters polarized muons with a beam energy of $E_{\mu} = 160$ GeV off the deuterons in a polarized ^{6}LiD solid-state target corresponding to a c.m.s. energy of $\sqrt{S} \simeq 18$ GeV. On average the beam polarization is $\mathcal{P}_{\mu} \simeq 76\%$, and about $\mathcal{F}_d \simeq 50\%$ of the deuterons can be polarized with an average polarization of $\mathcal{P}_d \simeq 50\%$ [15].

Hadrons can be detected if their scattering angle is less than $\theta_{\max} = 70$ mrad in the laboratory frame. This acceptance was recently upgraded to $\theta_{\max} = 180$ mrad for all future runs. In the event selection for a "high-p_{T}" sample, the charged hadrons have to pass further cuts [20]: the invariant mass $m(H_c, H_d)$ of the two produced hadrons has to be larger than 1.5 GeV, and the sum of the transverse momenta squared must obey $p_{\mathrm{T},c}^2 + p_{\mathrm{T},d}^2 > 2.5\ \mathrm{GeV}^2$ with both $p_{\mathrm{T},c}$ and $p_{\mathrm{T},d}$ larger than 0.7 GeV. In addition, the fractions $z_{c,d}$ of the parent parton's momenta carried by the detected hadrons $H_{c,d}$ are chosen to be $z_{c,d} > 0.1$.

The maximal virtuality of the quasi-real photons in (7) is taken to be $Q^2_{\max} = 0.5\ \mathrm{GeV}^2$. The fraction y of the lepton's momentum taken by the photon is restricted to be in the range $0.1 \le y \le 0.9$. We note that the often omitted non-logarithmic pieces in (7) result in a small but non-negligible contribution for the muons.

Figure 2 shows the dependence of both the unpolarized and polarized LO photoproduction cross section (3) on the unphysical factorization/renormalization scales varied in the range $(p_{\mathrm{T},c}^2 + p_{\mathrm{T},d}^2)/4 \le \mu^2 \le 4(p_{\mathrm{T},c}^2 + p_{\mathrm{T},d}^2)$. Both cross sections exhibit a very large scale dependence, which is, however, not uncommon for LO estimates. Sets of polarized parton densities with a moderate gluon polarization like GRSV "standard" result in an almost vanishing cross section as the two "direct" subprocesses, photon–gluon fusion and QCD-Compton scattering, cancel each other almost entirely; see also Fig. 4 and the discussions be-

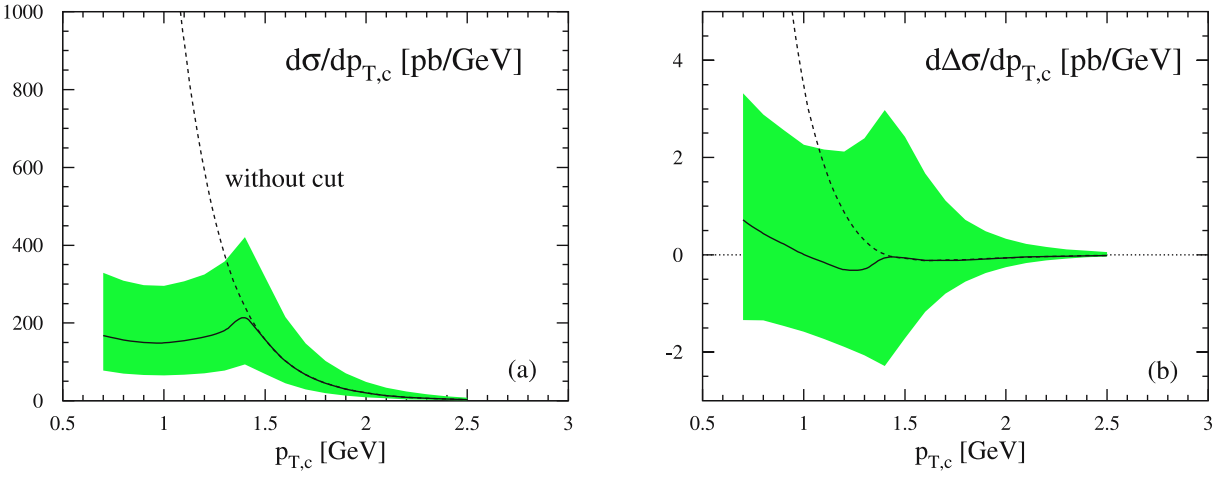

Fig. 2. Scale dependence of the unpolarized **a** and polarized **b** photoproduction cross section for two charged hadrons at LO for COMPASS with $\theta_{\max} = 70$ mrad. The scales in (3) are varied simultaneously in the range $(p_{\mathrm{T},c}^2 + p_{\mathrm{T},d}^2)/4 \le \mu^2 \le 4(p_{\mathrm{T},c}^2 + p_{\mathrm{T},d}^2)$ as indicated by the *shaded bands*. The *solid lines* correspond to the default choice where $\mu^2 = p_{\mathrm{T},c}^2 + p_{\mathrm{T},d}^2$. The *dotted lines* show the impact of lifting the experimental cut $p_{\mathrm{T},c}^2 + p_{\mathrm{T},d}^2 > 2.5\ \mathrm{GeV}^2$

low. Even the sign of the polarized cross section cannot be determined within the scale uncertainty here. As always, the computation of the relevant NLO QCD corrections is a mandatory task as theoretical uncertainties associated with the residual scale dependence are due to the truncation of the perturbative series at a given order and are expected to decrease significantly beyond the LO approximation. Such a calculation for hadron-pair production is a formidable task and still not complete at present [26].

From a recent calculation of the NLO QCD corrections to spin-dependent, *single-inclusive* photoproduction of high-$p_{\rm T}$ hadrons [51] we know though that theoretical scale uncertainties are only marginally reduced, if at all, at the NLO level at c.m.s. energies relevant for COMPASS and HERMES. This is in sharp contrast to what one generally expects and what indeed happens at collider energies; see, e.g., [52, 53]. In addition, the NLO corrections in [51] turned out to be sizable and different for the polarized and unpolarized cross sections, thus affecting also the spin asymmetries defined in (9). Clearly, this underpins the delicacy of perturbative calculations in the fixed-target regime, i.e., for small c.m.s. energies and transverse momenta of only a few GeV. Before drawing any conclusions about the hadronic spin structure, in particular Δg from measurements of the spin asymmetries $A_{\rm LL}$, one has to demonstrate the applicability of pQCD methods first. For this purpose, an important "benchmark" would be the comparison of the relevant unpolarized cross sections with theoretical expectations, e.g., given in Fig. 2a. Unfortunately, such a kind of information is still lacking from COMPASS for the time being. Let us stress that a possible discrepancy between experiment and theory at moderate c.m.s. energies would not necessarily imply that standard pQCD methods are beyond remedy. It would only call for further improvements by resumming large terms in the perturbative series, for instance, threshold logarithms, to all orders in the strong coupling. This is known to lead often to a much improved agreement between data and pQCD calculations; see, e.g., [54, 55].

The dotted lines in Fig. 2a,b correspond to the unpolarized (a) and polarized (b) cross sections computed without imposing the experimental cut of $p_{{\rm T},c}^2 + p_{{\rm T},d}^2 > 2.5\,{\rm GeV}^2$. This cut, which ensures hard scattering, is responsible for the cusp observed around $p_{{\rm T},c} \simeq 1.4\,{\rm GeV}$ and for the significant reduction of the cross section for smaller $p_{{\rm T},c}$.

Figure 3 shows our expectations for the double-spin asymmetry $A_{\rm LL}$, (9), at LO based on the cross sections shown in Fig. 2 for the default choice of scales. Apart from the "standard" set of GRSV polarized parton densities [46], we also use the three other sets, introduced at the beginning of Sect. 3, with very different assumptions about the gluon polarization. In the upper panel of Fig. 3 we study the importance of the "resolved" photon contribution to the photoproduction cross section (5). By comparing the experimentally relevant spin asymmetry for the sum of "direct" and "resolved" contributions (solid lines) with $A_{\rm LL}$ computed for the "direct" part alone (dashed lines), one can infer that, irrespective of the chosen Δg,

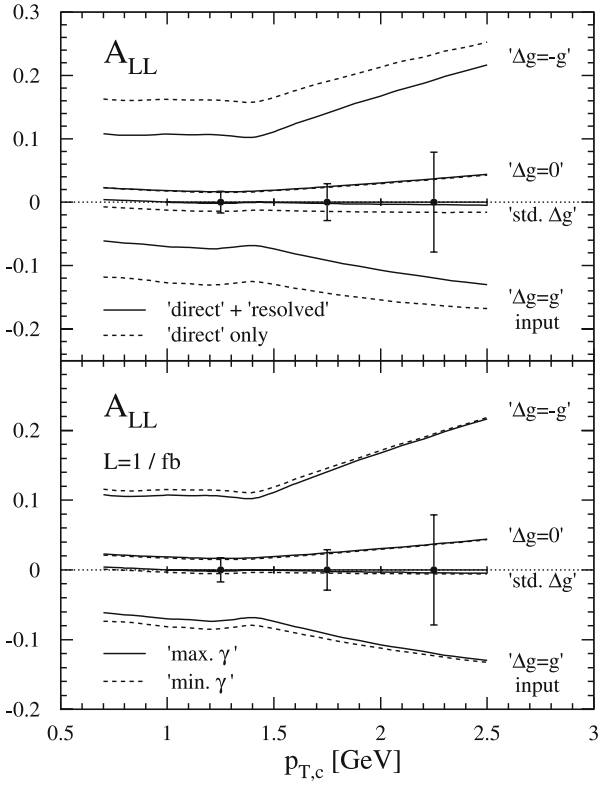

Fig. 3. Double-spin asymmetry $A_{\rm LL}$, (9), at LO for different gluon polarizations in the nucleon (see text). The *upper panel* shows the spin asymmetry with (*solid lines*) and without (*dashed lines*) including the "resolved" contribution. In the *lower panel* the dependence of $A_{\rm LL}$ on the two extreme photon scenarios, "maximal" (*solid lines*) and "minimal" saturation (*dashed lines*), is shown. The *error bars* indicate the estimated statistical accuracy for such a measurement at COMPASS in certain bins of $p_{{\rm T},c}$ based on an integrated luminosity of 1 fb^{-1}

the "resolved" part is non-negligible. It leads to a significant shift in the absolute value of the spin asymmetry, and neglecting it in the analysis would clearly lead to wrong conclusions about Δg.

The impact of the unknown, non-perturbative parton content of the circularly polarized photon on $A_{\rm LL}$ is examined in the lower panel of Fig. 3 by making use of the two extreme models [47–50] also introduced at the beginning of Sect. 3. As can be seen, the actual choice of the model barely affects the results for the spin asymmetry. Any difference between the two results diminishes further towards larger $p_{{\rm T},c}$. This can be readily understood as the photonic parton densities are probed on average at medium-to-large momentum fractions x_γ. In this region the partonic content of the photon is dominated by the "point-like" contribution which is independent of the details of the unknown non-perturbative input [47–50]. Certainly, this finding somewhat simplifies the theoretical analysis of the spin asymmetry in terms of Δg.

Figure 3 also demonstrates that the double-spin asymmetry $A_{\rm LL}$ is sensitive to different model assumptions for the gluon polarization. A large and positive gluon polarization yields a sizable negative asymmetry, whereas a large

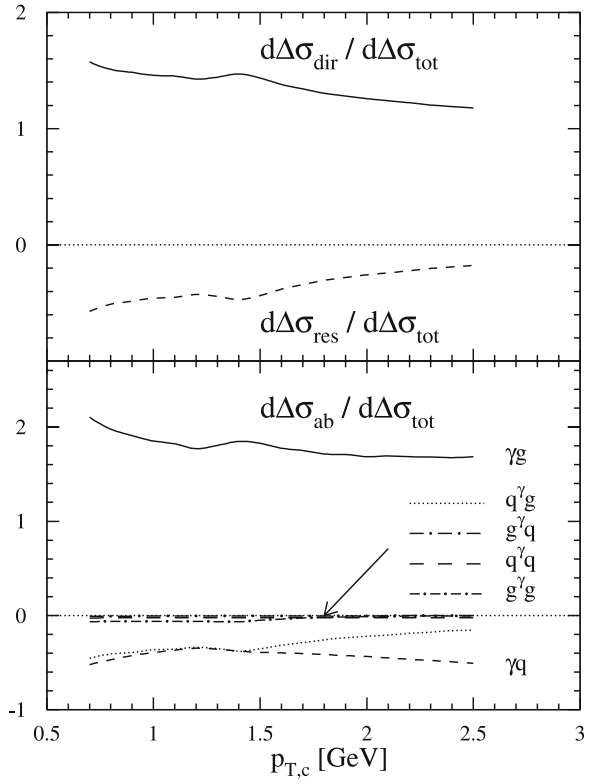

Fig. 4. The *upper panel* shows the "direct" and "resolved" contribution to the experimentally relevant polarized cross section. The *lower panel* shows the fractional contributions of the different partonic LO channels $a+b \to c+d$ to the photoproduction cross section

and negative Δg leads to a positive asymmetry. For the "standard" set of GRSV or when $\Delta g = 0$ is imposed at the input scale of the evolution we find asymmetries close to 0. To judge whether a measurement of $A_{\rm LL}$ can be actually turned into a constraint on Δg, we estimate the expected statistical accuracy $\delta A_{\rm LL}$ for COMPASS in certain bins of $p_{{\rm T},c}$, calculated from

$$\delta A_{\rm LL} \simeq \frac{1}{\mathcal{P}_\mu \mathcal{P}_d \mathcal{F}_d} \frac{1}{\sqrt{\sigma_{\rm bin}\mathcal{L}}}\,. \qquad (10)$$

Here, $\sigma_{\rm bin}$ denotes the unpolarized cross section integrated over the bin considered and $\mathcal{L}$ the integrated luminosity for which we assume $\mathcal{L} = 1\,{\rm fb}^{-1}$. All other quantities are as specified at the beginning of Sect. 3. Clearly, the region of $1 < p_{{\rm T},c} < 2\,{\rm GeV}$ is the most promising one to obtain information about the gluon polarization. At higher $p_{{\rm T},c}$'s the achievable statistical precision deteriorates as the cross section drops steeply with $p_{{\rm T},c}$.

First experimental results [20] find that the spin asymmetry (integrated also over $p_{{\rm T},c}$ for the time being) is close to 0. From this measurement a value of $\Delta g/g = 0.024 \pm 0.089({\rm stat.}) \pm 0.057({\rm sys.})$ at $x = 0.095 + 0.08\,(-0.04)$ and scale $\mu^2 = 3\,{\rm GeV}^2$ was extracted with the help of "purities", i.e., a "signal-to-background" separation based on Monte-Carlo simulations [20]. Compared to our theoretical expectations in Fig. 3 the COMPASS result of $A_{\rm LL} \simeq 0$ [20] is consistent with a moderate gluon polarization like in the GRSV "standard" set. However, as discussed above, one should take this result with a grain of salt unless an unpolarized reference cross section becomes available from COMPASS to verify the applicability of pQCD methods. In particular, one has to exclude that the observed smallness of the spin asymmetry is due to the presence of large non-perturbative effects. If these are spin-independent they would naturally lead to $A_{\rm LL} \simeq 0$ irrespective of Δg.

Next we turn to a closer analysis of how the results in Figs. 2 and 3 can be understood. To this end we study the different contributions to the polarized photoproduction cross section separately as illustrated in Fig. 4. The upper and lower panel show the fractional contributions of ${\rm d}\Delta\sigma_{\rm dir}$ and ${\rm d}\Delta\sigma_{\rm res}$ and of the different partonic LO channels $a+b \to c+d$, respectively. Here we use the maximal positive gluon polarization of GRSV with $\Delta g = g$ at the input scale, for which the cancellation between the photon–gluon fusion and QCD Compton subprocesses mentioned above is less relevant. For our "default" gluon polarization used in Fig. 2b the polarized cross section has a node at some $p_{{\rm T},c}$ such that the ratios are difficult to visualize. From Fig. 4 one infers that the "direct" part dominates in absolute value in the entire $p_{{\rm T},c}$-range shown and that the "resolved" and "direct" contributions have opposite signs. Turning to the individual subprocesses in the lower panel of Fig. 4 we note that the QCD Compton γq-channel always gives a positive contribution to the cross section[1] whereas the sign of the photon–gluon fusion channel is anti-correlated with the sign of Δg and its relevance scales with the magnitude of the unknown gluon polarization. This leads to a partial cancellation between the two "direct" channels for positive gluon polarizations, which explains the smallness of the polarized cross section for the GRSV "standard" gluon observed in Fig. 2b. Of the "resolved" processes only the scattering of a quark with large momentum fraction in the photon off a gluon in the nucleon makes a significant contribution, other channels are negligible. We note that in the unpolarized case (not shown here) all contributions to the cross section are positive with the "direct" part accounting for 80 percent or more.

We also wish to comment on the momentum fractions x_b predominantly probed in the nucleon in a measurement of hadron-pair photoproduction at COMPASS. For the unpolarized cross section this can be easily specified by looking at the distribution in x_b for a given bin of $p_{{\rm T},c}$. For example, for $p_{{\rm T},c}$ around 1 GeV we find $\langle x_b \rangle = 0.12 \pm 0.05$ which is consistent with the x-range estimated by COMPASS [20]. However, similar estimates for the polarized cross section and hence for $\Delta g/g$ are impossible without knowing Δg beforehand, as both the polarized cross sections and the helicity parton distributions are not positive definite. The relevance of contributions of opposite sign to the cross section strongly depends on the gluon polarization and completely obscures the meaning of an

[1] ${\rm d}\Delta\sigma_{\rm tot} < 0$ for the large and positive gluon polarization used in Fig. 4 such that ${\rm d}\Delta\sigma_{\gamma q}/{\rm d}\Delta\sigma_{\rm tot} < 0$.

averaged $\langle x_b \rangle$ here. This issue can be only consistently resolved in a future global analysis of polarized parton densities.

Next it is interesting to check whether the upgrade of the angular acceptance of the COMPASS experiment to $\theta_{\max} = 180\,\text{mrad}$ will enhance their sensitivity to Δg. In Fig. 5 we present our expectations for the double-spin asymmetry A_{LL} as a function of the transverse momentum $p_{\text{T},c}$ of one of the hadrons. Except for $\theta_{\max} = 180\,\text{mrad}$ all other settings and cuts are the same as in Fig. 3. The statistical precision for such a measurement is again estimated with the help of (10) for an integrated luminosity of $1\,\text{fb}^{-1}$. From the upper panel of Fig. 5 one infers that the "resolved" contribution modifies the asymmetry even more significantly than for $\theta_{\max} = 70\,\text{mrad}$. Even worse, there is now also a strong dependence on the model used to describe the parton content of the circularly polarized photon as can be seen in the lower panel of Fig. 5. This can be readily understood by noticing that due to the larger angular coverage one now probes the partonic structure of the photon also at momentum fractions x_γ where the details of the unknown non-perturbative input do matter. Only in the high-$p_{\text{T},c}$ region, where $x_\gamma \to 1$, the dependence on the model for Δf^γ becomes small. Clearly, a viable strategy would be to analyze data with different cuts on $\theta_{\max}$ or for bins in θ and to learn as much as possible about Δg first. Data up to $\theta_{\max} = 180\,\text{mrad}$ might then be used for studying the non-perturbative structure of circularly polarized photons. Needless to mention again that the validity of the pQCD framework for two-hadron production at COMPASS has to be confirmed prior to studies of A_{LL}.

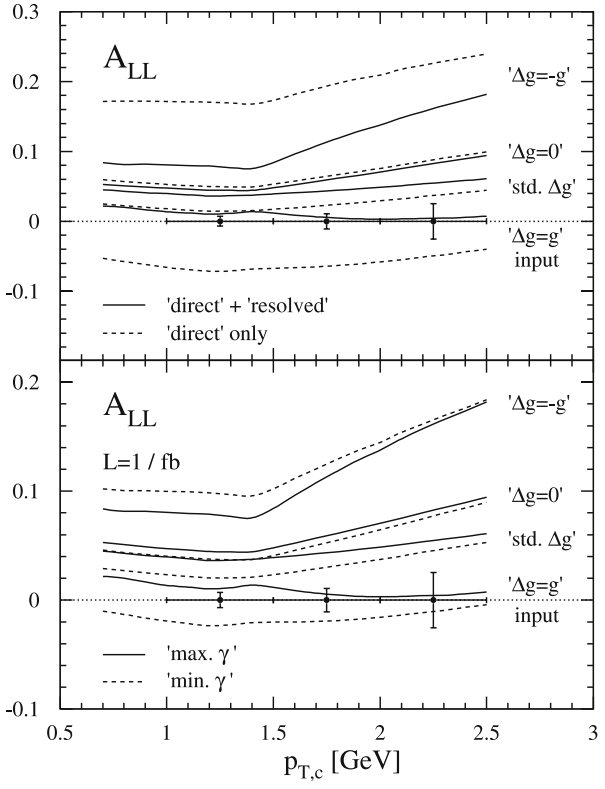

Fig. 5. As in Fig. 3 but now for the improved angular acceptance of $\theta_{\max} = 180\,\text{mrad}$

3.2 Two-hadron production at HERMES

At the HERMES experiment at DESY longitudinally polarized electrons/positrons with a beam energy of $E_e \simeq 27.5\,\text{GeV}$ were scattered off both a polarized deuterium or a polarized hydrogen gas target. The available c.m.s. energy of about $\sqrt{S} \simeq 7.5\,\text{GeV}$ is lower than at COMPASS, which even further limits the range of accessible transverse momenta. On average the lepton beam polarization is $\mathcal{P}_e \simeq 53\%$. For the polarization of the gas target we take $\mathcal{P}_d \approx \mathcal{P}_p \simeq 85\%$, and, contrary to a solid-state target, there is no dilution, i.e., $\mathcal{F}_p = \mathcal{F}_d = 1$.

We concentrate on phenomenological studies for a polarized deuterium target in line with the data sample with the highest statistics in the HERMES spin physics program which came to an end recently. The HERMES experiment has an angular acceptance of $40\,\text{mrad} \leq \theta_{\text{lab}} \leq 220\,\text{mrad}$ for hadrons. For all our numerical studies we demand a transverse momentum of at least 1 GeV for both detected hadrons $H_{c,d}$. We choose a maximal photon virtuality of $Q^2_{\max} = 0.1\,\text{GeV}^2$ in (7) and restrict y to $0.2 \leq y \leq 0.9$. The fractions of the parent parton's momenta carried by the produced hadrons are $z_{c,d} \geq 0.1$. Again, all scales in (3) are set equal to $\mu^2 = p^2_{\text{T},c} + p^2_{\text{T},d}$ unless stated otherwise.

Figure 6 shows the dependence of both the unpolarized and polarized LO photoproduction cross section, (3), on the unphysical factorization/renormalization scales varied in the range $(p^2_{\text{T},c} + p^2_{\text{T},d})/4 \leq \mu^2 \leq 4(p^2_{\text{T},c} + p^2_{\text{T},d})$. Not unexpectedly, due to the smaller c.m.s. energy of the HERMES experiment, the scale dependence is even larger than for COMPASS; cf. Fig. 2. All remarks about potential problems with the applicability of perturbative methods at fixed-target energies and the need for unpolarized "benchmark" cross sections also apply here.

Next we consider the corresponding double-spin asymmetry A_{LL} in Fig. 7. As in Fig. 3 we study the relevance of the "resolved" photon contribution in the upper panel and the dependence on models for the non-perturbative partonic structure of circularly polarized photons in the lower panel of Fig. 7. Estimates of the statistical accuracy, (10), are based on the integrated luminosity of $\mathcal{L} = 200\,\text{pb}^{-1}$ actually collected by HERMES and the parameters as specified above. Here, the "resolved" photon processes cause a much less pronounced shift in the asymmetry than for COMPASS; see Fig. 3. Also, there is almost no difference between the results obtained with the two extreme models for the Δf^γ densities. This is because for the same transverse momentum $p_{\text{T},c}$ the HERMES experiment is closer to the end of phase-space than COMPASS, i.e., $x_{\text{T},c} = 2p_{\text{T},c}/\sqrt{S}$ is closer to 1. On average HERMES probes larger momentum fractions both in the nucleon and in the photon, which explains our results. Our estimates of the statistical accuracy in Fig. 7 are such that only the region $1 < p_{\text{T},c} < 1.5\,\text{GeV}$ is potentially useful to further constrain the gluon polarization Δg. New experimental results from HERMES for both A_{LL} and the underlying unpolarized

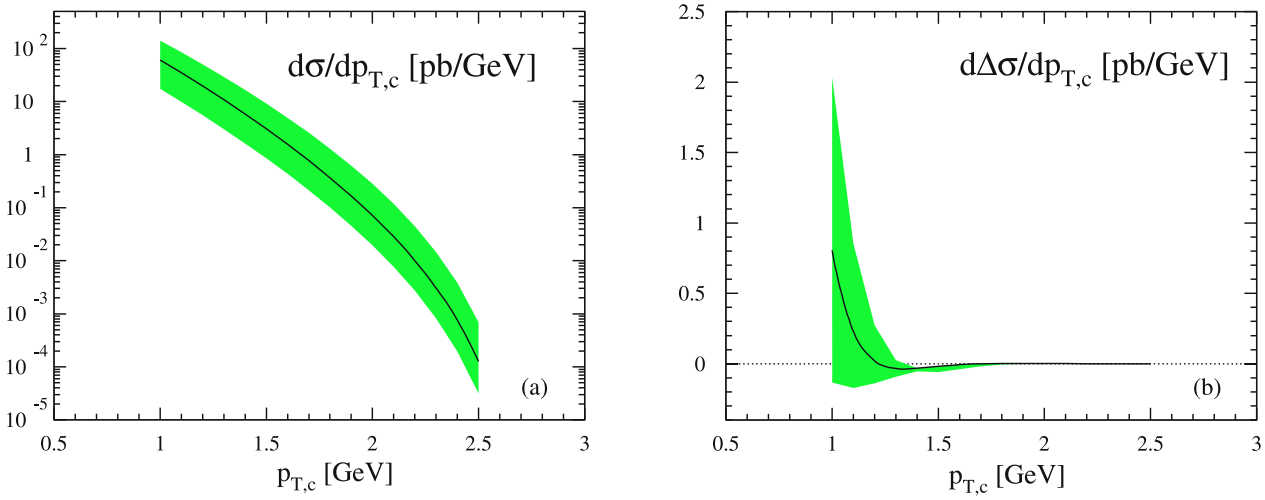

Fig. 6. Scale dependence of the unpolarized **a** and polarized **b** photoproduction cross section for two charged hadrons in LO for HERMES. The scales in (3) are varied simultaneously in the range $(p_{\mathrm{T},c}^2+p_{\mathrm{T},d}^2)/4 \le \mu^2 \le 4(p_{\mathrm{T},c}^2+p_{\mathrm{T},d}^2)$ as indicated by the *shaded bands*. The *solid lines* correspond to the default choice where $\mu^2 = p_{\mathrm{T},c}^2+p_{\mathrm{T},d}^2$

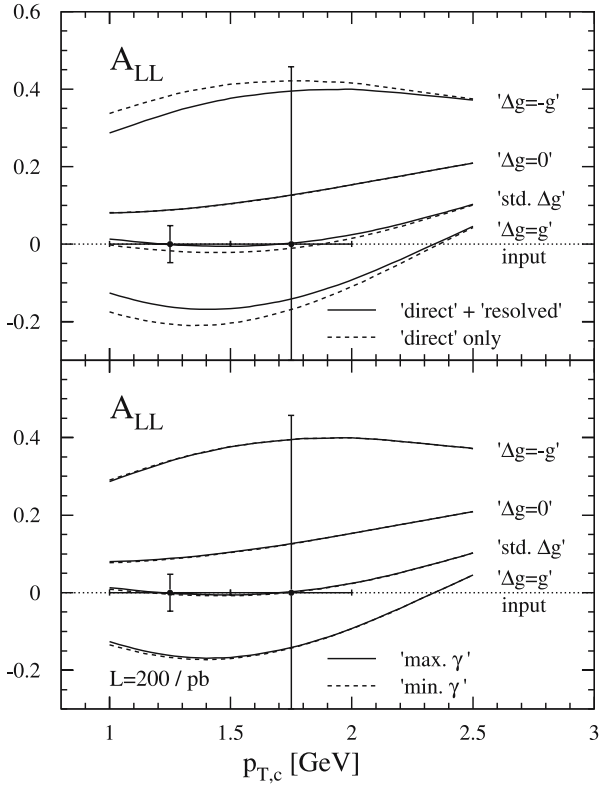

Fig. 7. As in Fig. 3 but know for HERMES kinematics (see text). Estimates of the statistical accuracy are based on an integrated luminosity of 200 pb^{-1}

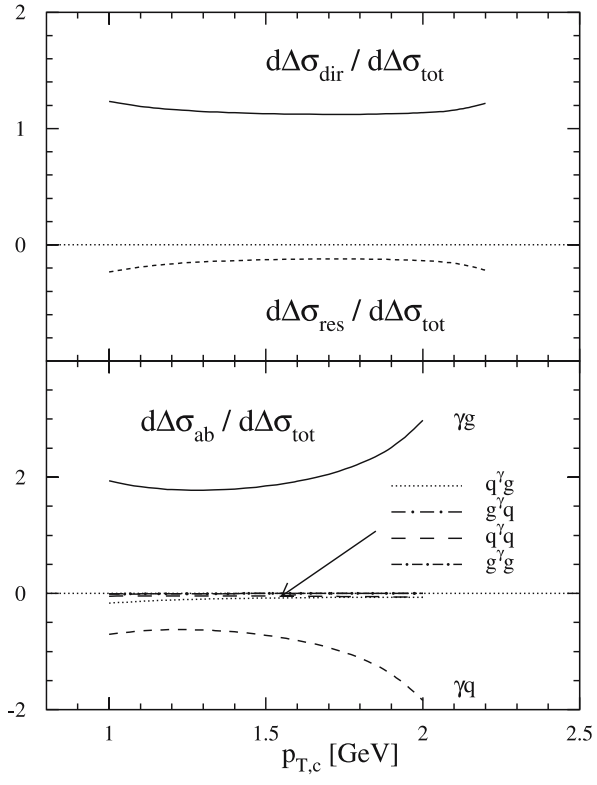

Fig. 8. As in Fig. 4 but now for HERMES kinematics (see text)

cross section will become available in the near future [56], superseding the results of an earlier publication [18].

We finish this section with a detailed study of the different contributions to the polarized photoproduction cross section. The upper and lower panel of Fig. 8 show the fractional contributions of $\mathrm{d}\Delta\sigma_{\mathrm{dir}}$ and $\mathrm{d}\Delta\sigma_{\mathrm{res}}$ and of the different partonic LO channels $a+b \to c+d$, respectively. As for Fig. 4 we use the maximal positive gluon polarization of GRSV with $\Delta g = g$ at the input scale. Again the choice is due to the fact that for our "default" gluon polarization, GRSV "standard", the cross section develops a node at some $p_{\mathrm{T},c}$, such that ratios are difficult to visualize. As is already expected from Fig. 7, the "resolved" photon cross section is fairly small throughout, though not com-

pletely negligible. Again it contributes with the sign opposite to the one of the "direct" cross section; cf. Fig. 4. As for COMPASS kinematics before, we observe a partial cancellation of the two "direct" channels: photon–gluon fusion and QCD Compton scattering. None of the four "resolved" contributions makes a significant contribution at LO.

3.3 Prospects for a future polarized *ep* collider

The most interesting option for a future experimental spin physics facility is a first polarized lepton–proton collider such as the eRHIC project at BNL [30, 31] currently under discussion. Here we consider the asymmetric collider option using the existing 250 GeV proton beam of RHIC and a new 10 GeV electron beam, i.e., a c.m.s. energy of $\sqrt{S} = 100$ GeV. The physics program of such a machine is based on the extensive and highly successful exploration of unpolarized *ep* collisions at the DESY-HERA collider. The determination of the gluon density from scaling violations in DIS down to very small x and establishing the concept of photonic parton densities in photoproduction processes are some of the many physics highlights of HERA.

From similar precision studies of scaling violations in polarized DIS at eRHIC it would be possible to access the gluon polarization down to $x \simeq 10^{-3}$, about one decade in x lower than in *pp* collisions at RHIC. In photoproduction processes it is expected that "resolved" contributions play a much more significant role at eRHIC than at fixed-target experiments [32]. This offers exciting prospects to learn about the Δf^γ densities, as was already demonstrated in case of single-inclusive pion photoproduction in [53].

Studies of hadron-pair production have the advantage that one has better control of the momentum fractions probed in the hadron and in the photon. For instance, by demanding a "trigger hadron" in the proton's forward direction and scanning the other hadron's rapidity one can select kinematical regions which are particularly sensitive to the non-perturbative structure of the photon. This is demonstrated in Fig. 9 where we give estimates for $A_{\rm LL}$ at $\sqrt{S} = 100$ GeV. The laboratory rapidity of the "trigger" hadron is integrated in the range $0.6 \le \eta_d \le 2.6$ and $2.6 \le \eta_d \le 3.6$ in the upper and lower panel, respectively, and the rapidity of the other hadron is left unintegrated. For $\eta_c \lesssim 0$ our results are fairly independent of the choice of a particular model for Δf^γ, while for $\eta_c \gtrsim 1$ the results strongly depend on Δf^γ. This is in particular the case if the trigger hadron is detected more forward in the incoming proton's direction, i.e., for $2.6 \le \eta_d \le 3.6$ (lower panel of Fig. 9). Note that in this subsection positive rapidities denote the proton direction, in line with common conventions usually used at HERA. Again this behavior can be understood by looking at the typical momentum fractions x_γ probed in (3): for $\eta_{c,d}$ large and positive one finds $x_\gamma \ll 1$, and for $\eta_{c,d}$ large and negative x_γ approaches 1.

We also give estimates for the statistical accuracy in Fig. 9 based on beam polarizations of $\mathcal{P}_{e,p} = 0.7$ and an integrated luminosity of 1 fb^{-1}. The latter is expected to be accumulated within only a few weeks of running eRHIC so that the statistical accuracy can be eventually much

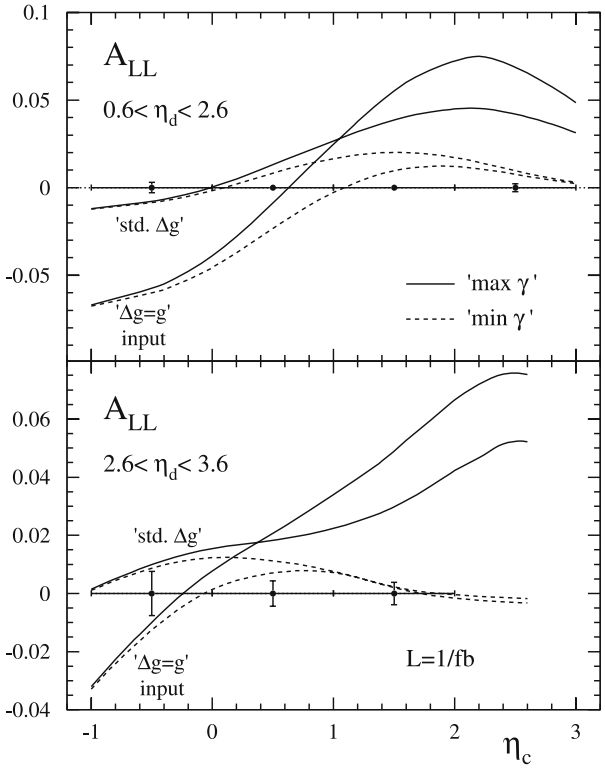

Fig. 9. Double-spin asymmetry for photoproduction of two charged hadrons in LO at $\sqrt{S} = 100$ GeV. Results are given for two different gluon polarizations of the nucleon and the two scenarios for the Δf^γ densities. Both hadrons are required to have a transverse momentum of at least 2 GeV. The laboratory rapidity of one of the hadrons is integrated in the range $0.6 \le \eta_d \le 2.6$ and $2.6 \le \eta_d \le 3.6$ in the *upper* and *lower panel*, respectively. Estimates of the statistical accuracy refer to an integrated luminosity of 1 fb^{-1}

better than the one shown in Fig. 9. In addition, we demand a minimum transverse momentum for both hadrons of 2 GeV and $z_{c,d} > 0.1$. For the equivalent photon spectrum in (7) we use similar parameters as the H1 and ZEUS experiments at HERA: $Q^2_{\rm max} = 0.5$ GeV^2, and the momentum fraction taken by the photon is limited to $0.2 \le y \le 0.85$. Note that the "boost" factor between the laboratory and the *ep* c.m.s. frame is very similar for the asymmetric collider option for eRHIC and for HERA.

Keeping in mind that the polarized gluon distribution Δg should be known fairly well in the range relevant in Fig. 9, i.e. $x \gtrsim 0.01$, from RHIC by the time eRHIC would start to operate, there are excellent prospects to study the so far unknown parton content of circularly polarized photons.

4 Conclusions

In summary, we have presented a phenomenological study of spin-dependent photoproduction of hadron pairs at c.m.s. energies relevant for the COMPASS and HERMES

experiments as well as for a possible future polarized *ep* collider. So far, our studies are limited to the LO approximation of QCD but will be amended to NLO accuracy in due time.

We have consistently included the "direct" and "resolved" photon contributions to the photoproduction cross section. It turned out that the "resolved" part leads to a significant shift in the experimentally relevant double-spin asymmetries and has to be accounted for in future analyses of the data. Fixed-target experiments are, however, mainly sensitive to the perturbative "pointlike" part of the photon structure. This simplifies attempts to extract the gluon polarization Δg, which is the main goal of COMPASS and one of the goals of HERMES. The non-perturbative parton content of circularly polarized photons can be probed in detail in photoproduction processes at higher c.m.s. energies, which hopefully will become available at some point in the future. By that time we most likely have a good knowledge of the spin structure of the nucleon, in particular from ongoing measurements at RHIC.

The double-spin asymmetries for both COMPASS and HERMES show the expected sensitivity to the gluon polarization in the nucleon. Keeping in mind the very sizable scale dependence at LO, all results for A_{LL} have to be taken with a grain of salt, unless the applicability of perturbative methods for two-hadron production at comparatively low transverse momenta and c.m.s. energies has been thoroughly investigated and demonstrated. This is best achieved by comparing the underlying unpolarized cross sections for the production of hadron pairs with theoretical expectations. If these checks are passed, the production of hadron pairs in lepton–nucleon collisions will be an interesting and complementary tool to further constrain the polarized gluon density at momentum fractions of about $x = 0.1$–0.2. If it turns out that data and theory do not match, these measurements will open up a window to study the effects of all-order resummations, the relevance of higher-twist corrections, and perhaps the transition to the non-perturbative regime so far little explored and understood.

Acknowledgements. We are grateful to E.C. Aschenauer, P. Liebing, and V. Mexner (HERMES) and to H. Fischer, S. Hedicke, F.-H. Heinsius and J.-M. Le Goff (COMPASS) for valuable discussions and information about the experimental details of their photoproduction measurements. C.H. was supported by a grant of the "Bayerische Eliteförderung". This work was supported in part by the "Deutsche Forschungsgemeinschaft (DFG)".

References

1. See, for example: K. Rith, in Proceedings of the 12th International Workshop on Deep Inelastic Scattering (DIS2004), Strbske Pleso, Slovakia, D. Bruncko et al. (eds.) (2004), p. 183
2. See, for example: R.L. Jaffe, A. Manohar, Nucl. Phys. B **337**, 509 (1990)
3. See, for example: G. Bunce, N. Saito, J. Soffer, W. Vogelsang, Ann. Rev. Nucl. Part. Sci. **50**, 525 (2000)
4. C. Aidala et al., Research Plan for Spin Physics at RHIC (2005), BNL report BNL-73798-2005
5. PHENIX Collaboration, S.S. Adler et al., Phys. Rev. Lett. **91**, 241 803 (2003)
6. PHENIX Collaboration, S.S. Adler et al., Phys. Rev. Lett. **95**, 202 001 (2005)
7. PHENIX Collaboration, S.S. Adler et al., Phys. Rev. D **71**, 071 102(R) (2005)
8. STAR Collaboration, J. Adams et al., Phys. Rev. Lett. **92**, 171 801 (2004)
9. STAR Collaboration, J. Adams et al., nucl-ex/0602011
10. STAR Collaboration, M.L. Miller, hep-ex/0604001, to appear in the Proceedings of the Particles and Nuclei International Conference (PANIC 05), Santa Fe, New Mexico, October 2005
11. PHENIX Collaboration, S.S. Adler et al., Phys. Rev. Lett. **93**, 202 002 (2004)
12. PHENIX Collaboration, S.S. Adler et al., Phys. Rev. D **73**, 091 102 (2006)
13. PHENIX Collaboration, K. Boyle, talk presented at the Particles and Nuclei International Conference (PANIC 05), Santa Fe, New Mexico, October 2005, to appear in the Proceedings
14. STAR Collaboration, B.I. Abelev et al., hep-ex/0608030
15. COMPASS Collaboration, G. Baum et al., CERN/SPSLC 96-14 (1996)
16. HERMES Collaboration, The HERMES Physics Program & Plans for 2001–2006, DESY-PRC, 2000
17. A. Bravar, D. von Harrach, A. Kotzinian, Phys. Lett. B **421**, 349 (1998)
18. HERMES Collaboration, A. Airapetian et al., Phys. Rev. Lett. **84**, 2584 (2000)
19. Spin Muon Collaboration (SMC), B. Adeva et al., Phys. Rev. D **70**, 012 002 (2004)
20. COMPASS Collaboration, E.S. Ageev et al., Phys. Lett. B **633**, 25 (2006)
21. E706 Collaboration, L. Apanasevich et al., Phys. Rev. Lett. **81**, 2642 (1998)
22. P. Aurenche et al., Eur. Phys. J. C **9**, 107 (1999)
23. P. Aurenche et al., Eur. Phys. J. C **13**, 347 (2000)
24. U. Baur et al., hep-ph/0005226
25. C. Bourrely, J. Soffer, Eur. Phys. J. C **36**, 371 (2004)
26. C. Hendlmeier et al., work in progress
27. M. Fontannaz, B. Pire, D. Schiff, Z. Phys. C **8**, 349 (1981)
28. J.J. Peralta, A.P. Contogouris, B. Kamal, F. Lebessis, Phys. Rev. D **49**, 3148 (1994)
29. G. Grispos, A.P. Contogouris, G. Veropoulos, Phys. Rev. D **62**, 014 023 (2000)
30. See http://www.bnl.gov/eic for information concerning the eRHIC/EIC project, including the "whitepaper", BNL-report 68933, Feb. 2002
31. A. Deshpande, R. Milner, R. Venugopalan, W. Vogelsang, Ann. Rev. Nucl. Part. Sci. **55**, 165 (2005)
32. M. Stratmann, W. Vogelsang, Z. Phys. C **74**, 641 (1997)
33. S.B. Libby, G. Sterman, Phys. Rev. D **18**, 3252 (1978)
34. R.K. Ellis, H. Georgi, M. Machacek, H.D. Politzer, G.G. Ross, Phys. Lett. B **78**, 281 (1978)
35. R.K. Ellis, H. Georgi, M. Machacek, H.D. Politzer, G.G. Ross, Nucl. Phys. B **152**, 285 (1979)
36. D. Amati, R. Petronzio, G. Veneziano, Nucl. Phys. B **140**, 54 (1980)

37. D. Amati, R. Petronzio, G. Veneziano, Nucl. Phys. B **146**, 29 (1978)
38. G. Curci, W. Furmanski, R. Petronzio, Nucl. Phys. B **175**, 27 (1980)
39. J.C. Collins, D.E. Soper, G. Sterman, Phys. Lett. B **134**, 263 (1984)
40. J.C. Collins, D.E. Soper, G. Sterman, Nucl. Phys. B **261**, 104 (1985)
41. J.C. Collins, Nucl. Phys. B **394**, 169 (1993)
42. D. de Florian, S. Frixione, Phys. Lett. B **457**, 236 (1999)
43. B.A. Kniehl, G. Kramer, B. Pötter, Nucl. Phys. B **582**, 514 (2000)
44. CTEQ Collaboration, J. Pumplin et al., JHEP **0207**, 012 (2002)
45. M. Glück, E. Reya, A. Vogt, Phys. Rev. D **46**, 1973 (1992)
46. M. Glück, E. Reya, M. Stratmann, W. Vogelsang, Phys. Rev. D **63**, 094 005 (2001)
47. M. Glück, W. Vogelsang, Z. Phys. C **55**, 353 (1992)
48. M. Glück, W. Vogelsang, Z. Phys. C **57**, 309 (1993)
49. M. Glück, M. Stratmann, W. Vogelsang, Phys. Lett. B **337**, 373 (1994)
50. M. Stratmann, W. Vogelsang, Phys. Lett. B **386**, 370 (1996)
51. B. Jäger, M. Stratmann, W. Vogelsang, Eur. Phys. J. C **44**, 533 (2005)
52. B. Jäger, A. Schäfer, M. Stratmann, W. Vogelsang, Phys. Rev. D **67**, 054 005 (2003)
53. B. Jäger, M. Stratmann, W. Vogelsang, Phys. Rev. D **68**, 114 018 (2003)
54. See, e.g., D. de Florian, W. Vogelsang, Phys. Rev. D **71**, 114 004 (2005) and references therein
55. See, e.g., D. de Florian, W. Vogelsang, Phys. Rev. D **72**, 014 014 (2005) and references therein
56. E.C. Aschenauer, P. Liebing, private communications